Dyes and Pigments 81 (2009) 187–192

Contents lists available at ScienceDirect

Dyes and Pigments

journal homepage: www.elsevier.com/locate/dyepig

Blue pigments based on $Co_xZn_{1-x}Al_2O_4$ spinels synthesized by the polymeric precursor method

Luiz K.C. de Souza [a], José R. Zamian [a], Geraldo N. da Rocha Filho [a], Luiz E.B. Soledade [b], Ieda M.G. dos Santos [b], Antonio G. Souza [b], Thomas Scheller [c], Rômulo S. Angélica [c], Carlos E.F. da Costa [a,*]

[a] Laboratório de Catálise e Oleoquímica, ICEN, UFPA, Belém, Pará, Brazil
[b] LACOM, Departamento de Química/CCEN, Universidade Federal da Paraíba, Campus I, CEP 58059-900, João Pessoa, PB, Brazil
[c] Universidade Federal do Pará, Centro de Geociência, Caixa Postal 1611, 66075-110 Belém, Pará, Brazil

ARTICLE INFO

Article history:
Received 30 May 2008
Received in revised form
15 September 2008
Accepted 17 September 2008
Available online 10 October 2008

Keywords:
Spinel
Polymeric precursor
Ceramic pigment
Chromophore elements
UV–vis
Colorimetric coordinates

ABSTRACT

The $Co_xZn_{1-x}Al_2O_4$ system ($x = 0$; 0.1; 0.3; 0.5; 0.7; 0.9 and 1) was synthesized by the polymeric precursor method and characterized by the techniques XRD, TG-DTA, IR, UV–vis and colorimetry. The XRD patterns displayed the characteristic peaks of the spinel structure and a good crystallinity. The DTA curves showed an exothermic peak corresponding to the enthalpy of the transition taking place at about 700 °C. The infrared spectra displayed vibrations at about 650, 550, 540, 520, 500, 490 cm^{-1}, which were ascribed to the spinel structure. The UV–vis spectra presented three bands at 550, 580 and 620 nm attributed to the Co^{2+} spin transitions in tetrahedral sites. The colorimetric data point out the formation of blue pigments, corresponding to highly negative values of b^*. The lightness, coordinate L^*, increases with the heat treatment temperature. These facts reveal that $Co_xZn_{1-x}Al_2O_4$ is a promising system that can be employed to obtain ceramic blue pigments.

1. Introduction

Spinel-type oxide materials have attracted a great deal of attention from scientists and industry leaders because of their relevant magnetic, refractory and semiconducting properties [1,2]. The spinel structure, featuring the general formula AB_2O_4 displays 64 tetrahedral sites and 32 octahedral sites, of which only 8 tetrahedral sites and 16 octahedral sites are occupied by the cations A^{2+} and B^{3+}, respectively. There are two ideal types of this structure: the first one is the normal spinel, in which the tetrahedral sites are occupied by the cations A^{2+} and the octahedral sites by the cations B^{3+}. The second ideal type is the inverse spinel, in which all the tetrahedral sites are occupied by cations B^{3+}, while an equal number of cations A^{2+} and B^{3+} share the octahedral sites [3,4]. Besides these ideal structures, spinels can display a partially inverted structure, moreover with the presence of a T-dependent cation. In this case the occupancy of tetrahedral and octahedral cations will shift toward a random distribution with increasing temperature [5].

Recently, a new application of the spinels as ceramic pigments has been explored, owing to their high mechanical resistance, high thermal stability, low temperature sinterability and the easy incorporation of chromophore ions into the spinel lattice, allowing for different types of doping, thus producing ceramic pigments with different colors [1–6].

Blue pigments are widely used in industry to bring color to plastics, paints, fibers, papers, rubbers, glass, cement, glazes, ceramics and porcelain enamels [7]. The main source of ceramic blue pigments is cobalt, in compounds such as Co_2SiO_4 (olivine), $(Co,Zn)_2SiO_4$ (willemite) and $CoAl_2O_4$ (cobalt spinel). But cobalt is scarce and expensive, thus increasing the production costs of cobalt-based ceramic pigments. Moreover, serious environmental problems may occur from the manufacturing process of Co-based ceramic pigments [6].

Therefore, the present paper aims at synthesizing ceramic blue pigments from the $Co_xZn_{1-x}Al_2O_4$ ($x = 0$; 0.1; 0.3; 0.5; 0.7; 0.9 and 1) system, synthesized by means of the polymeric precursor method. Gouveia et al. [8], Kakihana [9] and Lessing [10] provide a description and discussion of such synthesis method. The $Co_xZn_{1-x}Al_2O_4$ system allows for a reduction of the production costs and also for minimizing the environmental damage, as the amount of Co is reduced.

Several methods can be employed for the synthesis of simple oxides or oxide-based systems. The most common methods are: solid state reaction [11], sol–gel [12], micro-emulsion [4], co-precipitation

* Corresponding author. Tel./fax: +55 91 32017364.
E-mail address: emmerson@ufpa.br (C.E.F. da Costa).

0143-7208/$ – see front matter © 2008 Elsevier Ltd. All rights reserved.
doi:10.1016/j.dyepig.2008.09.017

[13], hydrothermal [14] and polymeric precursor method [9,10,15]. This latter method should be emphasised as it offers important advantages in relation to other chemical methods, such as: low cost, as the reagents used in large scale are relatively cheap, oxide synthesis at low temperatures, good chemical homogeneity at the molecular level of all the components and accurate stoichiometric control, even in complex systems [9,10,15].

2. Experimental section

The polymeric precursor method consists in the formation of a polymer in which the metal cations are homogeneously distributed within the polymer chain, aiming at a better cation distribution in the final oxide product. The metal cations were chelated with citric acid, an α-hydroxycarboxylic acid. Later, the metal chelates react with ethylene glycol, a polyhydric alcohol, in order to occur the polyester formation. A better description and discussion of this method is provided by Gouveia et al. [8], Kakihana [9], Lessing [10]. The $Co_xZn_{1-x}Al_2O_4$ ($x = 0$; 0.1; 0.3; 0.5; 0.7; 0.9 and 1) system was synthesized using the aforementioned polymeric precursor method.

The reagents utilized are cobalt acetate ($C_4H_6CoO_4 \cdot 4H_2O$), zinc nitrate ($Zn(NO_3)_2 \cdot 6H_2O$), aluminum nitrate ($Al(NO_3)_3 \cdot 9H_2O$), citric acid (CA) and ethylene glycol (EG). The (CA)/metal molar ratio was of 3:1, while the (CA)/(EG) mass ratio was of 60:40. Initially aluminum nitrate was dissolved in distilled water under constant stirring, later citric acid and then cobalt acetate and zinc nitrate were added. After being kept at around 70 °C for 1 h, ethylene glycol was added. A gel was obtained, and it undertook a preliminary heat treatment for 2 h at a temperature of 350 °C in an air atmosphere. Such heat treatment leads to a partial degradation of the organic structure and its expansion, due to the gas liberation during the combustion. Thus the powder precursor is formed, a fragile and black material. Next the powder precursor is deagglomerated and suffers the final heat treatment, eliminating the remaining organic matter, at the temperatures of 600, 700, 800 and 900 °C.

The XRD patterns were determined in an X'PERT PRO MPD (PW3040/60) diffractometer, from PANalytical, with a ceramic X-ray tube (λ Cu $K_{\alpha 1} = 1.540598$ Å), model PW3373/00, 2200 W, 60 kV. The following analysis conditions were used: voltage (kV): 40; current (mA): 40; scan range (5°–100°); step size (0.02°); scan mode: continuous; counting time (s): 5; divergence slit: slit fixed 1/2°; mask fixed: 10 mm; anti-scatter slit: slit fixed 1°; sample movement type: spinning; rotation time (s): 1.0. The Rietveld method was applied by the softwave Fullprof. The crystallite size was calculated by the means of the Scherrer equation.

The infrared spectra of the powders were taken in an IR 100 model Thermo-Nicolet equipment, in the 4000–400 cm^{-1} region. The TG–DTA thermal analyses were performed in a Thermal Sciences device coupled to a STA 1500 simultaneous thermal analyzer from Stantan Redcroft, in an air atmosphere, using a mass sample of about 10 mg, in the temperature interval from 25 to 1000 °C, with a heating rate of 10 °C min^{-1}. The CIELab chromatic coordinates as well as the UV–vis absorption spectra were taken by means of a Gretac Macbeth Color-eye 2180 colorimeter, using a D65 illumination, which is similar to daylight.

3. Results and discussion

Fig. 1 depicts the XRD patterns of the samples from the $Co_xZn_{1-x}Al_2O_4$ system heat treated at 800 °C. At this temperature for all the values of x studied, the characteristic peaks of the spinel structure were noticed, according to the ICDD files 74-1136 and 82-2252, for $ZnAl_2O_4$ and $CoAl_2O_4$, respectively. The patterns did not show the presence of secondary phases.

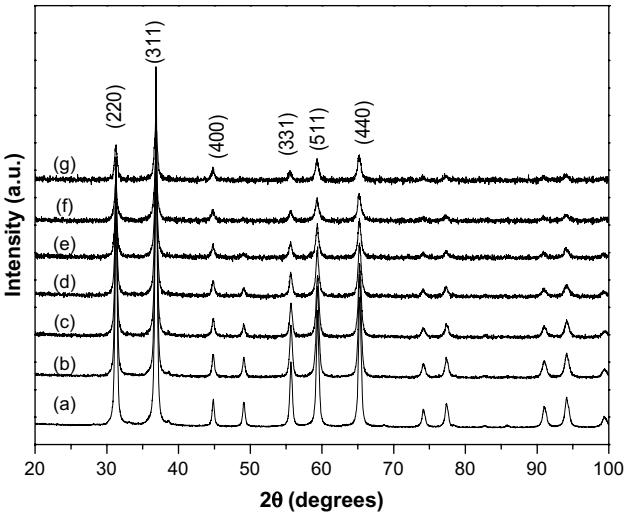

Fig. 1. XRD diffraction patterns of the following powder samples, heat treated at 800 °C (a) $ZnAl_2O_4$, (b) $Co_{0.1}Zn_{0.9}Al_2O_4$, (c) $Co_{0.3}Zn_{0.7}Al_2O_4$, (d) $Co_{0.5}Zn_{0.5}Al_2O_4$, (e) $Co_{0.7}Zn_{0.3}Al_2O_4$, (f) $Co_{0.9}Zn_{0.1}Al_2O_4$ and (g) $CoAl_2O_4$.

The development of the spinel phase at a relatively low temperature indicates one advantage of this synthesis route, as compared with other methods. For instance, Melo et al. [16] prepared $CoAl_2O_4$ by solid state reaction, obtaining such phase at a temperature of about 1000–1200 °C.

In the present work, the Rietveld refinement of XRD data, Fig. 1, allowed calculating the values of lattice parameter and crystallite size of the $Co_xZn_{1-x}Al_2O_4$ system, heat treated at 800 °C, Fig. 2.

Accompanying the increasing tendency shown in the theoretical values for the lattice parameters of $ZnAl_2O_4$ (8.05 Å) and $CoAl_2O_4$ (8.106 Å), the experimental values of lattice parameters and unit cell volume gradually increase upon the Co-substitution from zinc, from 8.083 Å to 8.095 Å in the case of lattice parameter, and from 528.10 $Å^3$ to 530.45 $Å^3$ in the case of unit cell volume. Such raise in the unit cell is in agreement with the values from ICDD files, Fig. 1. It should be stressed that the formation of a nanocrystalline structure, with the further reduction in the mean crystallite size upon the Co-enrichment, diminishing its value from 38.1 nm to 22 nm. It should be remarked that these two properties fairly obey Végard's law reasonably closely, with the corresponding linear relationship of lattice parameter and crystallite size with the Co-enrichment of the system, Fig. 2.

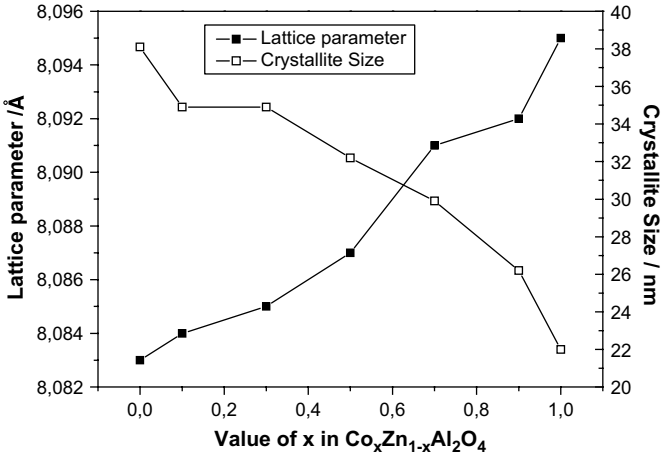

Fig. 2. Lattice parameter and crystallite size of $Co_xZn_{1-x}Al_2O_4$ ($x = 0$; 0.1; 0.3; 0.5; 0.7; 0.9 and 1), heat treated at a 800 °C, as a function of the Co amount.

Fig. 3 depicts the XRD patterns for the sample $Co_{0.5}Zn_{0.5}Al_2O_4$ heat treated at different temperatures. The results indicate that higher temperatures promote the increase of the system crystallinity. The patterns also show that the spinel phase is formed at 600 °C, according to the ICDD (International Centre for Diffraction Data) files 74-1136 and 82-2252, respectively for $ZnAl_2O_4$ and $CoAl_2O_4$.

Fig. 4 shows the TG curves of the powder precursors from the $Co_xZn_{1-x}Al_2O_4$ system. These curves suggest that the decomposition occurs in two steps. The first one results from the exit of water and gases adsorbed on the surface of the powder precursor. The second step is attributed to the combustion of the organic matter. The first step accounts for about 20%, the second for roughly 60%, summing up around 80% of total mass loss.

The DTA curves are illustrated in Fig. 5, which shows an endothermic peak at about 100 °C, corresponding to the energy adsorbed during the processes of water evaporation and de-sorption of gases from the surface of the precursor powders. Another peak, a strong exothermic peak, ascribed to the combustion of the organic matter is noticed at about 340 °C for most of the samples, but is shifted to around 430 °C for the samples $CoAl_2O_4$ and $ZnAl_2O_4$. A second and weaker peak, whose attribution was not determined, was clearly noticed at about 710 °C, only for the samples $CoAl_2O_4$ and $ZnAl_2O_4$. The crystallization of these compounds in the spinel phase is not accompanied by a mass loss. This fact was also reported by Duan et al. [17] for the synthesis of $ZnAl_2O_4$ by a new sol–gel method, with the authors reporting also an exothermic peak, centered at 450 °C, which corresponds to a crystallization temperature.

The exothermic peaks for extreme samples $ZnAl_2O_4$ and $CoAl_2O_4$ are smaller than for the samples containing both Zn and Co. This fact might be related to a smaller reactivity of these aforementioned samples, as was also observed in the TG curves, see Fig. 4, in which the temperature needed for 50% of mass loss was significantly lower for the samples containing both Zn and Co.

Fig. 6 shows the infrared spectra of the $Co_xZn_{1-x}Al_2O_4$ system heat treated at 900 °C. In these spectral vibrations corresponding to the spinel structure are identified at about 650, 550, 540, 520, 500, 490 cm^{-1}. According to Dhak and Pramanik [18], the spinels display stretching bands in the 500–900 cm^{-1} range, associated with the vibrations of metal–oxygen, aluminum–oxygen and metal–oxygen–aluminum. The bands at 520 and 540 cm^{-1} are ascribed to the (ZnO_4), (CoO_4) and [AlO_6] vibrations, in agreement with Chen et al. [19], who identified the bands related to the tetrahedral

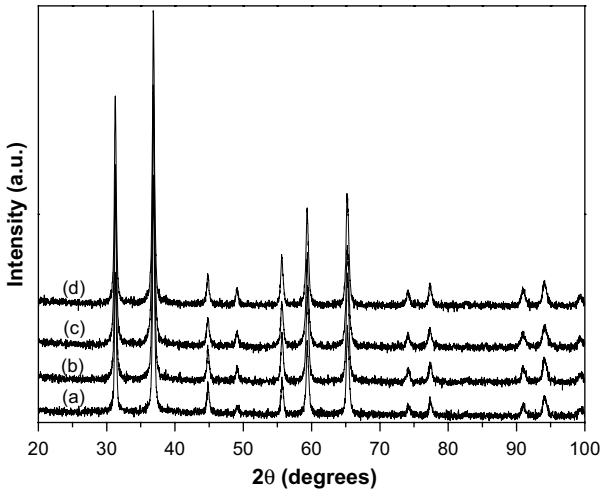

Fig. 3. XRD diffraction patterns of $Co_{0.5}Zn_{0.5}Al_2O_4$ heat treated at different temperatures, (a) 600 °C, (b) 700 °C, (c) 800 °C and (d) 900 °C.

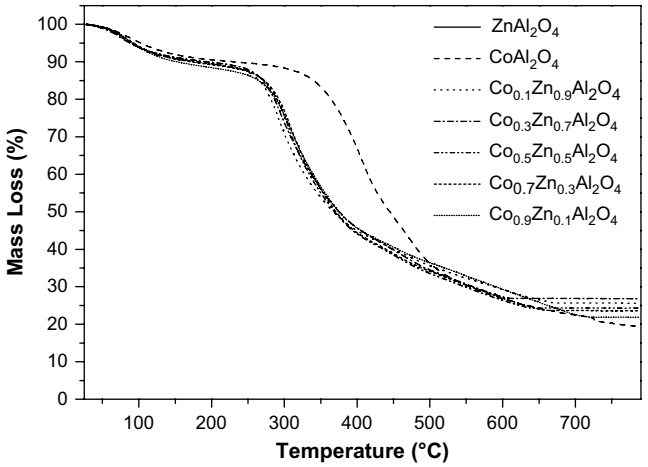

Fig. 4. TG curves of the system $Co_xZn_{1-x}Al_2O_4$ ($x = 0$; 0.1; 0.3; 0.5; 0.7; 0.9 and 1).

(CoO_4) groups and octahedral [AlO_6] groups. The band at about 650 cm^{-1} is related to the vibration of the group (ZnO_4). This band decreases its intensity as the amount of Co increases, pointing out the Co-occupation of the tetrahedral sites.

Stangar et al. [20] studied normal and Co-deficient $CoAl_2O_4$ thin films, observed only bands at about 670 cm^{-1}, 560 cm^{-1} and 510 cm^{-1}, which were ascribed to ($Co^{2+}O_4$) and [AlO_6] groups. Meyers et al. [21], investigating $CoAl_2O_4$ powders, observed that the Al–O and Co–O stretching frequencies are found in the range 900–470 and 550–340 cm^{-1}, respectively, whereas the Al–O–Co frequencies were noted in the 450–800 cm^{-1} region.

Therefore, due to the preferential occupancy of octahedral sites by Al and tetrahedral sites by Co and Zn, the $Co_xZn_{1-x}Al_2O_4$ system will not favor the presence of octahedral Co, neither Co^{2+} nor Co^{3+}. In spite of this, Meyer et al. [21] ascribed the two Al–O stretching bands, observed in the infrared spectra of $CoAl_2O_4$ powders at the range 500–900 cm^{-1}, to different oxygen-coordination states of Al atoms [AlO_6] and (AlO_4).

Fig. 7 illustrates the UV–vis absorbance spectra of the samples $Co_xZn_{1-x}Al_2O_4$ ($x = 0$; 0.1; 0.3; 0.5; 0.7; 0.9 and 1) powders heat treated at 900 °C. For all the samples can be noticed a strong absorption in the range from 540 nm to 630 nm, corresponding to the absorption of the colors yellow, orange and red. Thus, the reflectance occurs in the complementary colors, namely violet, blue and cyan, centered in the blue.

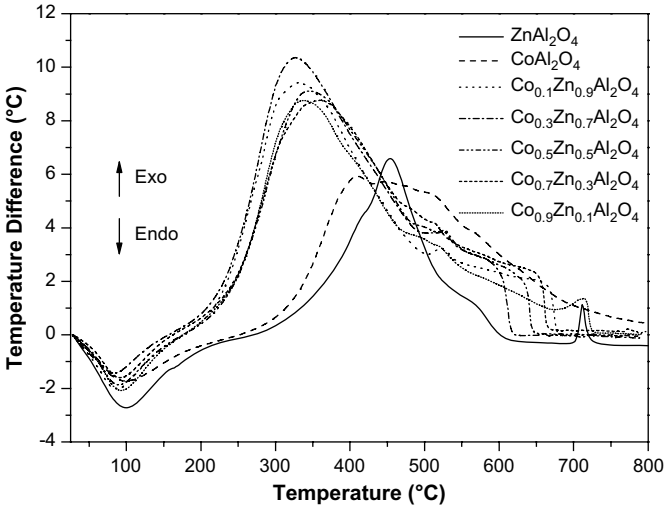

Fig. 5. DTA curves of the system $Co_xZn_{1-x}Al_2O_4$ ($x = 0$; 0.1; 0.3; 0.5; 0.7; 0.9 and 1).

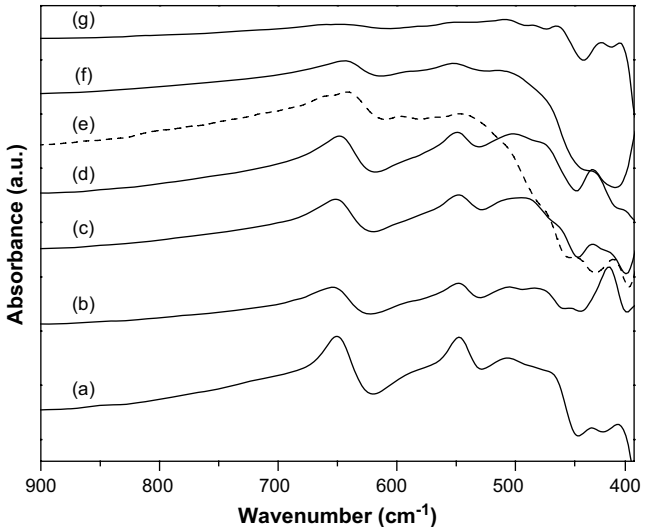

Fig. 6. Infrared spectra of (a) $ZnAl_2O_4$, (b) $Co_{0.1}Zn_{0.9}Al_2O_4$, (c) $Co_{0.3}Zn_{07}Al_2O_4$, (d) $Co_{0.5}Zn_{0.5}Al_2O_4$, (e) $Co_{0.7}Zn_{0.3}Al_2O_4$, (f) $Co_{0.9}Zn_{0.1}Al_2O_4$ and (g) $CoAl_2O_4$ heat treated at 900 °C.

Fig. 8 depicts the absorbance spectra of the sample $Co_{0.5}Zn_{0.5}Al_2O_4$ heat treated at 600, 700, 800 and 900 °C. For all of the samples a strong absorption in the range from 570 nm to 630 nm is apparent which corresponds to the absorption of the colors yellow, orange and red. Thus, the reflectance occurs in the complementary colors, namely violet, blue and cyan, centered in the blue.

It was verified that the bands at 478 nm, besides being influenced by the Co content, are also influenced by the heat treatment temperature. These data suggest that the Co^{2+} ions were incorporated within the $ZnAl_2O_4$ structure, replacing the Zn^{2+} ions in the tetrahedral sites.

The ions Co^{2+} present a $3d^7$ configuration and can occupy, besides other possibilities, tetrahedral and octahedral sites in spinel-type structures. For such ions there are, in the UV–vis region, three spin-allowed and three spin-forbidden electronic transitions, ascribed to $^4A_2(F) \rightarrow {}^4T_1(P)$ and $^4A_2(F) \rightarrow {}^2T(G)$, respectively [20,22].

In Fig. 8 are shown three bands, namely bands I, II and III, centered at approximately 550, 580 and 620 nm, respectively,

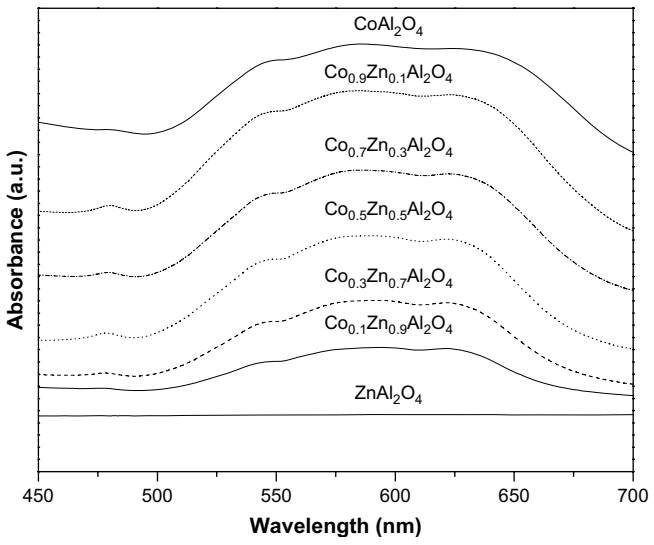

Fig. 7. UV–vis absorbance spectra of $Co_xZn_{1-x}Al_2O_4$ ($x = 0$; 0.1; 0.3; 0.5; 0.7; 0.9 and 1) heat treated at 900 °C.

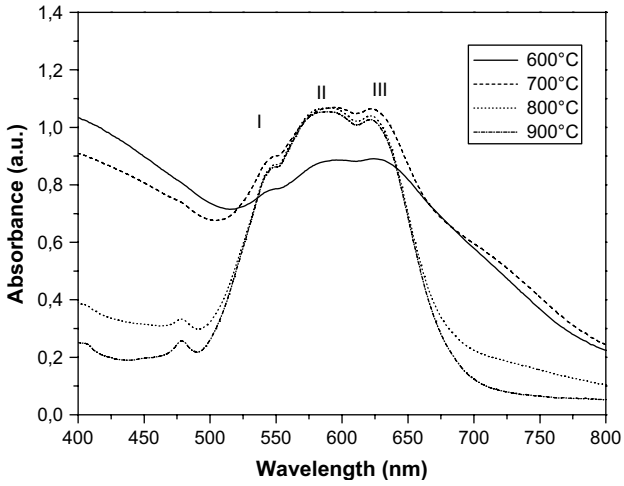

Fig. 8. UV–vis absorbance spectra of $Co_{0.5}Zn_{0.5}Al_2O_4$ heat treated at 600, 700, 800 and 900 °C.

which are attributed to the spin-allowed $^4A_2(F) \rightarrow {}^4T_1(P)$ transition of the Co^{2+} ions in tetrahedral sites. As the heat treatment temperature increases, these bands are better defined. Similar results were obtained by Stangar et al. [20].

Stangar et al. [20] investigating Co-deficient $CoAl_2O_4$ thin films, with a Co/Al molar ratio of 0.3, observed UV–vis transmittance bands with maxima at 544 nm, 580 nm and 625 nm. Zayat and Levy [22] also working with a Co-deficient $CoAl_2O_4$ samples, but in this case powders displaying the $Co_{0.75}Al_{2.25}O_4$ stoichiometry, reported the absorbance bands at 543 nm, 580 nm and 630 nm. Sales et al. [23] investigating powders with the composition $3(Al_{1.95}Co_{0.025}Ti_{0.025}O_3)\cdot 2SiO_2$, heat treated at 995 °C for 1 h, found peaks at 510 nm, 575 nm and 618 nm. The position of the bands I, II and III in the present paper, 550, 580 and 620 nm, generally agrees with the values disclosed in the literature [22,24].

In the present work, as already mentioned, another band is observed at around 478 nm, and it is assumed to be related to spin-forbidden transitions reported by Zayat and Levy [22]. Such a band is not observed for the sample treated at 600 °C. This fact agrees with the XRD patterns, which show that at 600 °C the sample $Co_{0.5}Zn_{0.5}Al_2O_4$ has a low crystallinity, but increases its long range ordering with the increase of the heat treatment temperature. Another possibility is the presence of a T-dependent cation ordering, in which the cooling might partially preserve the highly random high-temperature cation distribution [5]. In addition, Fig. 8 clearly evidences a ramp in the low wavelength part of the visible spectrum, suggesting the occurrence of charge transfer processes active in the samples treated at 600 and 700 °C.

Table 1
Values obtained from the deconvolution of the UV–vis absorbance spectra of $Co_{0.5}Zn_{0.5}Al_2O_4$ heat treated at different temperatures.

Temperature (°C)	Band	Center (nm)	Band intensity (a.u.)
600 ($r^2 = 0.9989$)	I	543.86	0.027
	II	590.51	0.168
	III	632.42	0.124
700 ($r^2 = 0.9991$)	I	541.01	0.085
	II	585.16	0.380
	III	631.41	0.265
800 ($r^2 = 0.9993$)	I	537.43	0.281
	II	584.21	0.761
	III	633.09	0.516
900 ($r^2 = 0.9993$)	I	536.15	0.332
	II	583.08	0.817
	III	632.80	0.584

Table 2
Colorimetric analysis of $Co_{0.5}Zn_{0.5}Al_2O_4$ heat treated at different temperatures.

Temperature (°C)	L^*	a^*	b^*
600	42.78	−6.57	3.82
700	42.77	−7.99	−3.32
800	46.48	−7.31	−27.64
900	47.47	−3.19	−36.24

In relation to the higher energy bands, thus displaying lower wavelengths, there are conflicting data in the literature. Zayat and Levy [22] reported that the peaks observed at 408 nm, 447 nm and 479 nm are related to the spin-forbidden $^4A_2(F) \rightarrow {}^2T(G)$ transition of the Co^{2+} ion in octahedral sites. On the other hand, Stangar et al. [20] considered that the bands whose wavelengths are below 520 nm are due to electronic transitions of Co^{3+} in octahedral sites. Sales et al. [23] observed a band at 480 nm, but they did not show its attribution.

Kim et al. [24] studied the $Co_{3-x}Fe_xO_4$ system and reported three visible peaks at 1.65 eV (752 nm), 2.4 eV (517 nm) and 2.8 eV (443 nm). The first peak was assigned to a $t_{2g}(Co^{3+}) \rightarrow t_2(Co^{2+})$ d–d charge transfer (CT) transition, from the $d(t_{2g})$ states of the octahedral Co^{3+} ion to the $d(t_2)$ states of the tetrahedral Co^{2+} ion.

It can be also noted that the increase of the heat treatment temperatures, leads to a decrease in the absorption, moreover at around 450 nm, what is related to the higher spinel crystallization, as pointed out in the XRD patterns of Fig. 3. This corresponds to an increase in the reflectance, thus leading to pigments with lighter blue hues, what agrees with higher values of the CIELab lightness, L^* coordinate, as will be later discussed. Similar results were obtained for the other samples, corresponding to other stoichiometries.

More detailed information on the bands in the range from 400 nm to 800 nm can be obtained from the deconvolution of these bands, for different temperatures, by employing the Peak Fit program, see Table 1. It was observed that the increase of the heat treatment temperature led to a shift of these bands toward a higher energy, in other words, toward a decrease in the absorbed wavelength, as it was reported by Stangar et al. [20].

The CIELab colorimetric coordinates allow for the quantitative and qualitative characterizations of the pigment colors. Table 2 shows these coordinates for the pigment $Co_{0.5}Zn_{0.5}Al_2O_4$, heat treated at different temperatures. It can be noticed that the increase of the heat treatment temperature practically does not oscillate the coordinate a^*. It slightly increases the lightness, L^*, whereas strongly decreases the coordinate b^*. Thus the pigment $Co_{0.5}Zn_{0.5}Al_2O_4$ calcined at 900 °C showed ab^* coordinate of −36.24, indicating a blue color, see Table 2, in agreement with the UV–vis spectra shown in Fig. 8. Similar results were obtained for other Co contents.

The chromatic coordinates (L^*, b^* and a^*) of the pigments $ZnAl_2O_4$, $Co_{0.1}Zn_{0.9}Al_2O_4$, $Co_{0.3}Zn_{0.7}Al_2O_4$, $Co_{0.5}Zn_{0.5}Al_2O_4$, $Co_{0.7}Zn_{0.3}Al_2O_4$, $Co_{0.9}Zn_{0.1}Al_2O_4$ and $CoAl_2O_4$, heat treated at 900 °C, are displayed in Table 3. It can be seen that the lightness, L^*, decreases with the increase of the Co content, pointing out the formation of darker pigments, in agreement with the UV–vis spectra, in Fig. 8.

Table 3
Colorimetric analysis of the samples heat treated at 900 °C.

Sample	L^*	a^*	b^*
$ZnAl_2O_4$	81.54	−0.42	0.54
$Co_{0.1}Zn_{0.9}Al_2O_4$	64.88	−8.89	−15.28
$Co_{0.3}Zn_{0.7}Al_2O_4$	54.88	−7.97	−25.78
$Co_{0.5}Zn_{0.5}Al_2O_4$	47.47	−3.19	−36.24
$Co_{0.7}Zn_{0.3}Al_2O_4$	48.04	−5.28	−24.32
$Co_{0.9}Zn_{0.1}Al_2O_4$	45.75	−2.31	−26.38
$CoAl_2O_4$	38.63	−3.28	−14.39

The coordinate a^* was kept negative for all the samples, indicating a slight green contribution, but showing an erratic oscillation. In terms of the b^* coordinate, it was kept highly negative for all the samples, with the tendency of showing the highest blue intensity for the medium level of Co content, but leading to a blue color for all the samples.

4. Conclusions

The system $Co_xZn_{1-x}Al_2O_4$ ($x = 0$; 0.1; 0.3; 0.5; 0.7; 0.9 and 1), in which the ion Co^{2+} is incorporated in the $ZnAl_2O_4$ spinel structure, thus gradually replacing the Zn^{2+} ions in the tetrahedral sites, was synthesized by the polymeric precursor method. Relatively low synthesis temperatures were employed, once the spinel phase was identified by XRD at 600 °C.

The infrared bands, according to the literature, were ascribed to (ZnO_4), (CoO_4) and [AlO_6] vibrations. The band attributed to the vibration of the group (ZnO_4) decreases its intensity as the amount of Co increases, pointing out the Co-occupation of the tetrahedral sites.

The UV–vis absorbance spectra of the samples $Co_xZn_{1-x}Al_2O_4$ display a strong absorption in the range from 540 nm to 630 nm, corresponding to the absorption of the colors yellow, orange and red. Thus, the reflectance occurs in the complementary colors, namely violet, blue and cyan, centered in the blue.

In these spectra are shown three bands, namely bands I, II and III, centered at approximately 550, 580 and 620 nm, respectively, which are attributed to the spin-allowed 4A2(F) → 4T1(P) transition of the Co^{2+} ions in tetrahedral sites. As the heat treatment temperature increases, these bands are better defined, in agreement with previously reported results.

The highly negative values of the b^* coordinate, obtained upon the substitution of Co^{2+} for Zn^{2+} ions point out that blue pigments were obtained. Higher Co-enrichment leads to darker blue pigments, with the tendency of obtaining the most negative values of b^* for the medium Co-enrichment levels.

These facts reveal that the system $Co_xZn_{1-x}Al_2O_4$ ($x = 0$; 0.1; 0.3; 0.5; 0.7; 0.9 and 1) can be employed to obtain ceramic blue pigments, of diverse hues, which offer potential industrial applications.

Acknowledgements

We Acknowledge the financial support from Universidade Federal do Pará (UFPA)-PIBIC.

References

[1] Lorenzi G, Baldi G, Benedetto DF, Faso V, Lattanzi P, Romanelli M. Spectroscopic study of a Ni-bearing gahnite pigment. Journal of the European Ceramic Society 2006;26:317–21.
[2] Fernández AL, Pablo L. Formation and the colour development in cobalt spinel pigments. Pigment and Resin Technology 2002;31(6):350–6.
[3] Sickafus KE, Wills JM. Structure of spinel. Journal of the American Ceramic Society 1999;82(12):3279–92.
[4] Giannakas AE, Ladavos AK, Armatas GS, Pomonis PJ. Surface properties, textural features and catalytic performance for NO + CO abatement of spinels MAl_2O_4 (M = Mg, Co and Zn) developed by reverse and bicontinuous microemulsion method. Applied Surface Science 2007;253:6969–79.
[5] Sepelak V, Becker KD. Comparison of the cation inversion parameter of the nanoscale milled spinel ferrites with that of the quenched bulk materials. Materials Science and Engineering A 2004;375–377:861–4.
[6] Llusar M, Forés A, Badenes JA, Calbo J, Tena MA, Monrós G. Colour analysis of some colbat-based blue pigments. Journal of the European Ceramic Society 2001;21:1121–30.
[7] Li W, Li j Guo J. Synthesis and characterization of nanocrystalline $CoAl_2O_4$ spinel powder by low temperature combustion. Journal of the European Ceramic Society 2003;23:2289–95.
[8] Gouveia DS, Soledade LEB, Paskocimas CA, Longo E. Color and structural analysis of $Co_xZn_{7-x}Sb_2O_{12}$ pigments. Materials Research Bulletin 2006;41:2049–56.

[9] Kakihana M. Sol–gel preparation of high temperature superconducting oxides. Journal of Sol–Gel Science and Technology 1996;6(1):7.
[10] Lessing PA. Mixed-cation oxide powders via polymeric precursors. American Ceramic Society Bulletin. 1989;68(5):1002–7.
[11] Suzuki T, Nagai H, Nohara M, Takagi H. Melting of antiferromagnetic ordering in spinel oxide $CoAl_2O_4$. Journal of Physics: Condensed Matter 2007;19. 145265 (5 pp).
[12] Vijaya JJ, Kennedy LJ, Sekaran G, Jeyaraj B, Nagaraja KS. Effect of Sr addition on the humidity sensing properties of $CoAl_2O_4$ composites. Sensors and Actuators B 2007;123:211–7.
[13] Britto S, Radha AV, Ravishankar N, Vishnu KP. Solution decomposition of the layered double hydroxide (LDH) of Zn with Al. Solid State Sciences 2007;9:279–86.
[14] Chen Z, Shi E, Zheng Y, Xiao B, Zhuang J. Hydrothermal synthesis of nanosized $CoAl_2O_4$ on $ZnAl_2O_4$ seed crystallites. Journal of the American Ceramic Society 2003;86(6):1058–60.
[15] Souza SC, Santos Img M, Silva RS, Cássia-Santos MR, Soledade LEB, Souza AG, et al. Influence of pH on iron doped Zn_2TiO_4 pigments. Journal of Thermal Analysis and Calorimetry 2005;79:451–4.
[16] Melo DMA, Cunha JD, Fernandes JDG, Bernardi MJ, Melo MAF, Martinelli AE. Evaluation of $CoAl_2O_4$ as ceramic pigments. Materials Research Bulletin 2003;38:1559–64.
[17] Duan X, Yuan D, Wang X, Xu H. Synthesis and characterization of nano-crystalline zinc aluminum spinel by a new sol–gel method. Journal of Sol–Gel Science and Technology 2005;35:221–4.
[18] Dhak D, Pramanik P. Particle size comparison of soft-chemically prepared transition metal (Co, Ni, Cu, Zn) aluminate spinels. Journal of the American Ceramic Society 2006;89(3):1014–21.
[19] Chen Z, Shi E, Li W, Aheng Y, Zhong W. Hydrothermal synthesis and optical property of nano-sized $CoAl_2O_4$ pigment. Materials Letters 2002;55:281–4.
[20] Stangar UL, Orel B, Krajnc M. Preparation and spectroscopic characterization of blue $CoAl_2O_4$ coatings. Journal of Sol–Gel Science and Technology 2003;26:771–5.
[21] Meyer F, Hempelmann R, Mathur S, Veith M. Microemulsion mediated sol–gel synthesis of nano-scaled MAl_2O_4 (M = Co, Ni, Cu) spinels from single-source heterobimetallic alkoxide precursors. Journal of Materials Chemistry 1999;9:1755–63.
[22] Zayat M, Levy D. Blue $CoAl_2O_4$ particles prepared by the sol–gel and citrate–gel methods. Chemistry of Materials 2000;12:2763–9.
[23] Sales M, Valentin C, Alarcón J. Cobalt aluminate spinel–mullite composites synthesized by sol–gel method. Journal of the European Ceramic Society 1997;17:41–7.
[24] Kim KJ, Kim HK, Park YR, Ahn GY, Kim CS, Park JY. Mössbauer and optical investigation of $Co_{3-x}Fe_xO_4$ thin films grown by sol–gel process. Hyperfine Interactions 2006;169:1363–9.